Pattern Recognition Letters 33 (2012) 991–999

Contents lists available at SciVerse ScienceDirect

Pattern Recognition Letters

journal homepage: www.elsevier.com/locate/patrec

# New iris recognition method for noisy iris images

Kwang Yong Shin [a], Gi Pyo Nam [a], Dae Sik Jeong [a], Dal Ho Cho [b], Byung Jun Kang [c], Kang Ryoung Park [a,*], Jaihie Kim [d]

[a] Division of Electronics and Electrical Engineering, Biometrics Engineering Research Center (BERC), Dongguk University, 26 Pil-dong 3-ga, Jung-gu, Seoul 100-715, Republic of Korea
[b] Dept. of Computer Science, Sangmyung University, 7 Hongji-dong, Jongno-gu, Seoul 110-743, Republic of Korea
[c] Technical Research Institute, Hyundai Mobis, 80-9, Mabuk-dong, Giheong-gu, Yongin-si, Gyeonggi-do 446-716, Republic of Korea
[d] School of Electrical and Electronic Engineering, Biometrics Engineering Research Center (BERC), Yonsei University, 134 Shinchon-dong, Seodaemun-gu, Seoul 120-749, Republic of Korea

ARTICLE INFO

*Article history:*
Available online 6 September 2011

*Keywords:*
Noisy iris images
Left or right eye
Color information
Textural information

ABSTRACT

When capturing an iris image under unconstrained conditions and without user cooperation, the image quality can be highly degraded by poor focus, off-angle view, motion blur, specular reflection (SR), and other artifacts. The noisy iris images increase the intra-individual variations, thus markedly degrading recognition accuracy. To overcome these problems, we propose a new iris recognition algorithm for noisy iris images. This research is novel in the following three ways compared to previous works. First, we propose the 1st step classification method which discriminates the "left or right eye" on the basis of the eyelash distribution and SR points. Since the iris pattern of the left eye differs from that of the right eye, the 1st step classification can enhance the accuracy of iris recognition. Second, the separability between intra- and inter-classes is increased by using the 2nd step classification based on the "color information" of the iris region. They are measured by using the Euclidean distance (ED), chi square distance (CSD), and hamming distance (HD) calculated with the color space models such as YIQ, YUV, YCbCr, HSI, and CMY. Third, "textural information" of the iris region is used for the 3rd step classification. That is, the 1-D Gabor filter is applied to the red, green, and gray image channels to afford three sets of iris codes from iris textures and, consequently, three HD scores, which are then combined on the basis of the weighted SUM rule to produce a final matching score.

The experimental results with the NICE.II training dataset (selected from UBIRIS.v2 database) showed that the decidability value ($d'$) was 1.6398 (the fourth-highest rank).


## 1. Short introduction

Among the various biometrics methods, iris recognition achieves particularly high recognition accuracy because the iris patterns between the pupil and sclera offer rich textures with a high degree of freedom (DOF) (Daugman, 1993, 2003, 2004). Most iris recognition systems currently available for personal identification require near-infrared (NIR) illumination, and they require user's cooperation to capture an iris image with good quality, which can give inconvenience to users. Thus, the challenge to improve the performance of iris recognition in an unconstrained environment has been issued (Proença and Alexandre, 2007).

Fig. 1 shows examples of noisy iris images, each affected by various factors such as low illumination; off-angle; rotation; blurring; and occlusion by the eyelids, that by eyelashes, noises by glasses, or occlusion by ghost regions. Since these factors reduce the similarity between intra-classes, the recognition performance is drastically degraded. In this research, new iris recognition method is proposed to improve the recognition performance for unconstrained image-acquisition environments. We propose the 1st step classification method which discriminates the "left or right eye" on the basis of the eyelash distribution and specular reflection (SR) points. And we use the 2nd step classification based on the "color information" of the iris region. Finally, the 3rd step relies on the "texture information" of the iris region for classification. That is, the 1-D Gabor filter is applied to the gray, red, and green channels to afford three separate iris codes and, consequently, three hamming distance (HD) scores, which are combined using the weighted SUM rule to produce a final matching score.

The remainder of the paper is organized as follows: Section 2 describes the proposed method. Section 3 describes the result analysis, and the conclusions are presented in Section 4.

* Corresponding author. Tel.: +82 2 2260 3329.
*E-mail addresses:* skyandla@dongguk.edu (K.Y. Shin), oscar1201@dongguk.edu (G.P. Nam), jungsoft97@dongguk.edu (D.S. Jeong), chodalho@msn.com (D.H. Cho), kangbyj@mobis.co.kr (B.J. Kang), parkgr@dongguk.edu (K.R. Park), jhkim@yonsei.ac.kr (J. Kim).

0167-8655/$ - see front matter 
doi:10.1016/j.patrec.2011.08.016

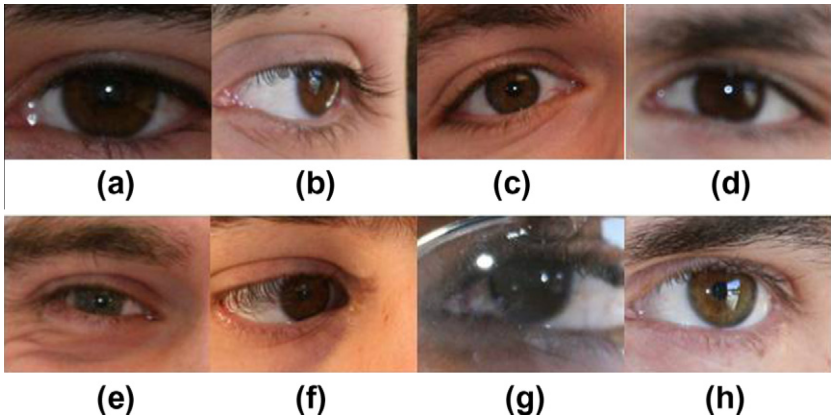


**Fig. 1.** The noisy iris images (NICE.II training dataset, 2009). (a) Low illumination. (b) Off-angle. (c) Rotation. (d) Blurring. (e) Occlusion by eyelids. (f) Occlusion by eyelashes. (g) Noises by glasses. (h) Occlusion by ghost region.

## 2. Description of the proposed method

### 2.1. Overview

Fig. 2 shows the overall procedure of the proposed method. It includes four steps: (I) iris region segmentation, (II) the 1st step classification of the "left or right eye", (III) the 2nd step classification using "color information" of iris region, and (IV) the 3rd step classification using "textural information" of iris region. The NICE.II contest focused on iris recognition, and so the results of iris segmentation were already provided, as shown in Fig. 3b. However, the pixel positions of the pupil and iris boundaries were not provided. So, in this research, the geometric center of black pixels (the result of iris segmentation of Fig. 3b) is calculated as a rough position of iris center. The rough radius of iris region is calculated based on the leftmost and rightmost positions of the black pixels. And, using the white pixels inside the black pixels of Fig. 3b, the accurate pupil center is determined. With the searching range based on the rough center position and rough radius of iris region, the accurate center position and radius of iris region are detected by circular edge detector (CED) (see "1" of Fig. 2 and Section 2.2) (Jeong et al., 2010).

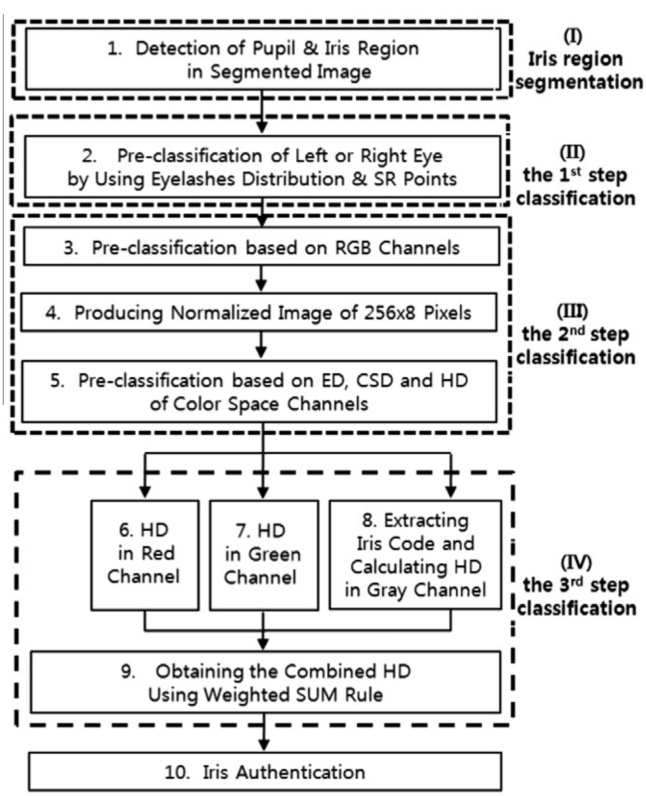


**Fig. 2.** Overall procedure of the proposed method.

Since the iris patterns of the left eye are different from those of right eye (Daugman, 2004), the accuracy of iris recognition can be enhanced by pre-classification of left or right eye image. In detail, the gray textural shapes of left iris are different from those of right iris. To prove it, in previous research (Daugman, 2004), he measured the distribution of hamming distance (HD) between left and right irises from any given person by using iris recognition algorithm based on gray textural information. For that, 648 left/right iris pairs from 324 persons were compared. Experimental results showed that the mean HD was 0.497 with standard deviation of 0.03108. And when the distribution of HD was measured from 9,060,003 different iris comparisons based on 4258 different iris images of different persons, the mean HD was 0.499 with standard deviation of 0.0317 (Daugman, 2004). By conclusion, the results with different irises (the mean: 0.499, the standard deviation: 0.0317) are almost similar to those with left/right irises (the mean: 0.497, the standard deviation: 0.03108), which represents that the patterns of left iris are different from those of right iris like different irises of different persons.

To discriminate the left or right eye, we use the eyelash distribution and specular reflection (SR) points (see "2" of Fig. 2 and Section 2.3). Eyelashes are differently distributed along the edges of the eyelid from the medial canthus to the lateral canthus, as shown in Fig. 4 (Na et al., 2006), and the more SR spots appear in the medial canthus than in the lateral canthus because of the lachrymal glands. The color information shown in Fig. 8 can be used to identify the human eye. So the second pre-classification step uses the proportion of the red (R), green (G), and blue (B) pixels to classify inter-class group of recognition (see "3" of Fig. 2 and Section 2.4).

After producing a normalized image of $256 \times 8$ pixels (see "4" of Fig. 2 and Section 2.5), the Euclidean distance (ED), chi square distance (CSD), and hamming distance (HD) between the input and enrolled images are calculated using the color space models such as RGB, YIQ, YUV, YCbCr, HSI, and CMY. These distance values are used to classify intra-class and inter-class groups (see "5" of Fig. 2 and Section 2.6). In general, brightness (gray) and color information are mixed in RGB and CMY space. However, the brightness and the color information are separated in YIQ, YUV, YCbCr, and

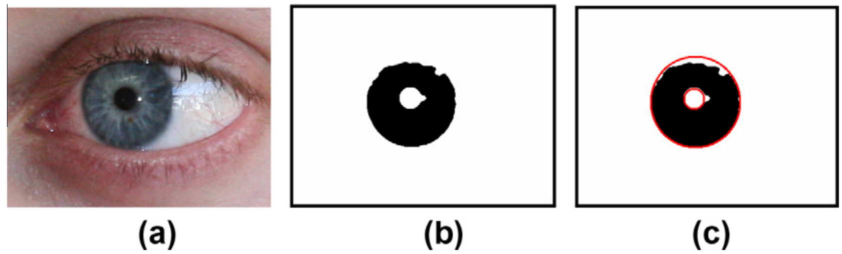


**Fig. 3.** Detection of pupil and iris boundaries. (a) Original image (NICE.II training dataset, 2009). (b) The segmented image provided by NICE.II contest (NICE.II training dataset, 2009). (c) Result of pupil and iris boundary detection.

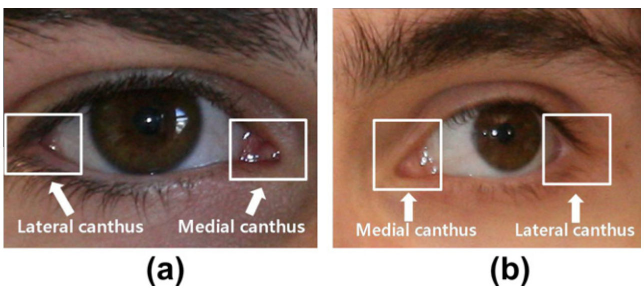


**Fig. 4.** Eyelash distribution and the SR on the medial canthus and lateral canthus. (a) "Right eye" image. (b) "Left eye" image.

HSI spaces (Gonzalez and Woods, 2002; Li and Drew, 2004). The color information of RGB and CMY are different from IQ, UV, CbCr and HS. And even the IQ, UV, CbCr and HS have different color characteristics each other (Gonzalez and Woods, 2002; Li and Drew, 2004). So, we can enhance the accuracy of iris recognition by using the various color spaces. Among Y of YIQ, YUV, YCbCr and I of HSI, only I of HSI is used for recognition.

The input iris images determined as imposter images by the 1st and 2nd classification steps are excluded from the genuine matching of the 3rd step classification. In addition, the threshold for classification between genuine and imposter distributions is established in the 1st and 2nd steps so genuine data is not classified as belonging to an imposter.

Then, iris codes are extracted by using the 1-D Gabor wavelet filter from the gray channel and the HD is calculated (see "8" of Fig. 2 and Section 2.7) (Park and Park, 2007). Since the two HDs from the red and green channels are already available in "5" of Fig. 2, the three HD scores for the red, green and gray channels are finally combined using the weighted SUM rule (see "9" of Fig. 2 and Section 2.8). The combined score is used to determine whether the input iris image is of the genuine or an imposter.

### 2.2. Detection of pupil and iris region

Since the NICE.II contest focused on iris recognition, the results of the iris segmentation are provided, as shown in Fig. 3b.

However, the pixel positions of the pupil and iris boundaries are not provided. So, in this research, the accurate centers and radii of pupil and iris regions are detected as follows.

The geometric center of black pixels (the result of iris segmentation of Fig. 3b) is calculated as a rough position of iris center. The rough radius of iris region is determined from the half of the difference between the rightmost and leftmost positions of the black pixels. As shown in Fig. 3b, the iris region has the gray value of 0 in the segmented image and the other areas have a gray value of 255. From this, we select the leftmost and rightmost positions at which the gray values change from 255 to 0 and 0 to 255, respectively.

The pupil center and radius are detected as follows. Using the white pixels inside the black pixels of Fig. 3b, component labeling is performed and one region (which includes the detected rough position of iris center) is regarded as a pupil area. With this pupil area, the geometric center is calculated as the accurate pupil center. Based on the rightmost and leftmost positions of this pupil area, the accurate pupil radius is obtained.

The accurate iris center and radius are detected as follows. With the searching range based on the detected rough center position and rough radius of iris region, the accurate center position and radius of iris region are detected by circular edge detector (CED) (Jeong et al., 2010):

$$\arg\max_{(x_0,y_0),r}\left[\frac{\partial}{\partial r}\left(\int_{-\frac{\pi}{4}}^{\frac{\pi}{6}}\frac{I(x,y)}{5\pi r/12}ds+\int_{\frac{5\pi}{6}}^{\frac{5\pi}{4}}\frac{I(x,y)}{5\pi r/12}ds\right)\right] \quad (1)$$

where $r$ is the radius of iris region. The coordinates $(x_0,y_0)$ denotes the center position of the iris region. By using the integro-differential operations of Eq. (1), the accurate center and radius of iris region are obtained (Jeong et al., 2010). The two integro-differential operations are done in the range of $-\frac{\pi}{4}\sim\frac{\pi}{6}$ radians and $\frac{5\pi}{6}\sim\frac{5\pi}{4}$ radians, respectively, as shown in Eq. (1). That is because the regions of the other ranges can be hidden by eyelids, which can cause the error of the integro-differential operations (Jeong et al., 2010). Fig. 3c shows the result of the detected pupil and iris boundaries.

### 2.3. The 1st step classification of the Left or Right eye

Eyelashes are differently distributed along the edge of the eyelid from medial canthus to lateral canthus as shown in Fig. 4 (Na et al., 2006). The medial canthus is the convergence point between the upper and lower eyelids on the lachrymal glands. The lateral canthus is the convergence point between the upper eyelid and lower eyelid on the opposite direction of the lachrymal glands. More eyelashes are observed in the lateral canthus than in the medial canthus, as shown in Fig. 4. In addition, more SR spots are observed in the medial canthus than in the lateral canthus because of the lachrymal glands. This can be used to distinguish between left and right eyes.

The original RGB image is converted into a grayscale image, as shown in Fig. 5a. Before measuring the eyelash distribution and detecting SR regions, the Retinex algorithm is used for illumination normalization (Nam et al., 2010); it can reduce illumination variation and enhance the distinctiveness of the original image. The image intensity $L(x,y)$ is expressed as (Nam et al., 2010):

$$L(x,y)=I(x,y)\times r(x,y) \quad (2)$$

where $I(x,y)$ and $r(x,y)$ denote the illumination component and the reflection ratio, respectively. The reflection ratio is a unique characteristic of an object regardless of the illumination, so eliminating the illumination component can reduce the illumination variation. Eq. (2) can be rewritten as Eqs. (3) and (4) (Nam et al., 2010).

$$\log L(x,y) = \log[I(x,y) \times r(x,y)] \tag{3}$$

$$\log r(x,y) = \log L(x,y) - \log I(x,y) \tag{4}$$

The illumination $I(x,y)$ is modeled as the convolution operation of an image $L(x,y)$ and the Gaussian filter $F(x,y)$. As shown in Eq. (5), the image has the effect of being more distinctive by subtracting the low-frequency component ($\log[L(x,y) * F(x,y)]$) from the image ($\log L(x,y)$) (Nam et al., 2010).

$$R(x,y) = \log r(x,y) = \log L(x,y) - \log(L(x,y) * F(x,y)) \tag{5}$$

$$F(x,y) = \frac{1}{2\pi\sigma^2} e^{-\frac{x^2+y^2}{2\sigma^2}} \tag{6}$$

where $R(x,y)$ denotes the Retinex image, and Fig. 5b shows the Retinex image of the original image of Fig. 5a. The consequent distinctiveness of eye region including iris and eyelashes is enhanced through the Retinex filtering. We compared the equal error rate (EER) of iris recognition when using the proposed Retinex filtering to that using conventional unsharp masking (Gonzalez and Woods, 2002). Experimental results showed the accuracy of iris recognition when using the Retinex filtering was better than that using unsharp masking.

The Retinex filtering is used for the following two objectives. First one is to enhance the distinctiveness of image, by which the measurement of eyelash distributions and detection of specular reflection (SR) are much easier for classifying the left and right iris images. Second one is to increase the distinctiveness of iris patterns, by which the accuracy of iris recognition is enhanced. For the first objective, the Retinex filtering is applied in the whole image. And the Retinex filtering is applied only in the iris region for the second objective.

According to the average diameters of the sclera and iris (Lefohn et al., 2003) and considering additional margin, we assume the maximum ratio of "half the length between the two corners of the eye" to "the iris radius" as being about 2.5. From this information, the horizontal width of the eyelash-searching region can be defined as shown in Fig. 6a.

More eyelashes along the upper eyelid are observed than the lower eyelid. In addition, the searching region for the eyelash in the vertical direction is determined based on the uppermost point of iris boundary and the middle point (between the iris center position and the lowermost point of the iris boundary) as shown in Fig. 6a.

The SR spots appear on the medial and lateral canthus regions, which are observed between the center position of the iris and the lowermost point of iris boundary in the vertical direction as shown in Fig. 7a. The searching region in the horizontal direction for detecting the SR is determined as shown in Fig. 7a.

Before discriminating between the "left eye" and "right eye" classes, we check the size of the searching region for the eyelashes. In case of severely off-angle images, the iris is close to the left or the right positions of the eye corners, as shown in Fig. 10a and b. To measure the correct distribution of the eyelashes, the size of the left searching region should be similar to that of the right searching region. It is difficult to discriminate the "left eye" and "right eye" classes in the small-sized searching regions of severely off-angle image, as shown in Fig. 10a and b. Therefore, this case is determined as "undetermined eye" class.

To discriminate the "left eye" and "right eye" classes, we measured two standard deviations (STD) ($\sigma_L$ and $\sigma_R$) of the pixel gray values in the left and right searching regions, respectively. The left and right searching regions are shown in Fig. 6a. If many eyelashes are included in the searching region, the STD becomes high as shown in Fig. 6b. The eyelashes are usually darker than the sclera and skin while the SRs are brighter than the sclera. If the gray level is lower than 40 in the eyelash-searching region of Fig. 6a, the point is determined as being an eyelash pixel. In addition, if the gray level is higher than 250 in the searching region for SRs in Fig. 7a, the point is determined as being an SR pixel. Fig. 6b and Fig. 7b show the detection result of eyelashes and SRs, respectively. The rules of determining the "right eye" and the "left eye" are represented as:

$$\begin{aligned}
&\text{“right eye”}, \quad \mathit{if}\ [(\sigma_L - \sigma_R \geqslant T_\sigma)\ \mathit{and}\ (D_L - D_R \geqslant T_D)]\ \mathit{or}\\
&[(N_L < N_R)\ \mathit{and}\ \{(0 < \sigma_L - \sigma_R < T_\sigma)\ \mathit{or}\ (0 < D_L - D_R < T_D)\}]\\
&\text{“left eye”}, \quad \mathit{if}\ [(\sigma_R - \sigma_L \geqslant T_\sigma)\ \mathit{and}\ (D_R - D_L \geqslant T_D)]\ \mathit{or}\\
&[(N_L > N_R)\ \mathit{and}\ \{(0 < \sigma_R - \sigma_L < T_\sigma)\ \mathit{or}\ (0 < D_R - D_L < T_D)\}]\\
&\text{“Undetermined eye”}, \quad \mathit{Otherwise}
\end{aligned} \tag{7}$$

where $\sigma_L$ and $\sigma_R$ denote the STDs in the left and right eyelash searching regions, respectively. In addition, the $D_L$ and $D_R$ represent the number of the detected eyelash pixels in the left and right eyelash searching regions, respectively. The $N_L$ and $N_R$ represent the

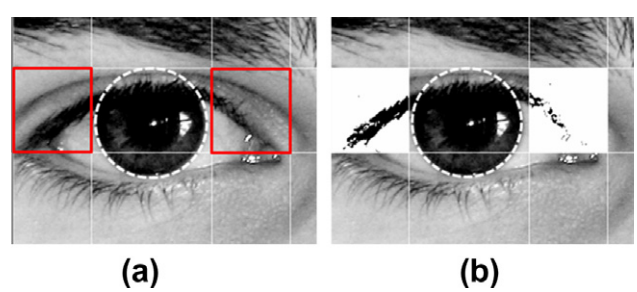


**Fig. 6.** Detection of eyelashes. (a) The searching regions for eyelashes. (b) The result of detecting eyelashes.

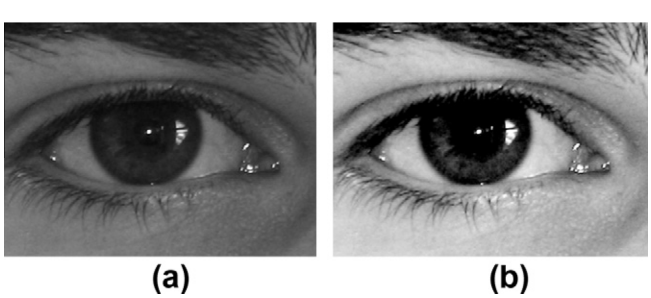


**Fig. 5.** An example of the illumination normalization. (a) Gray image of Fig. 4a. (b) Retinex image of (a).

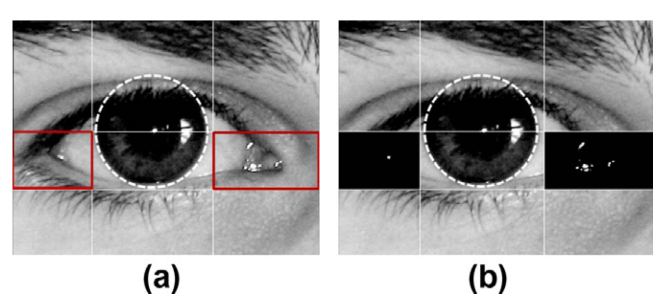


**Fig. 7.** Detection of SR. (a) The searching regions for SR. (b) The result of detecting SR.

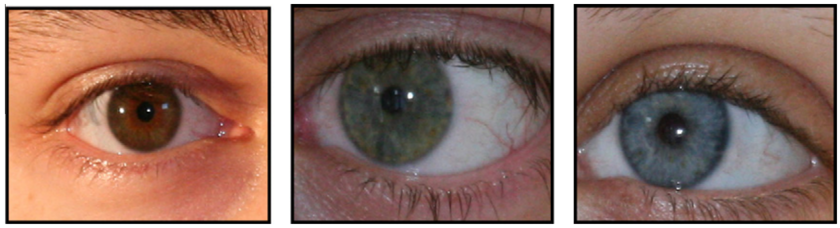

**Fig. 8.** Human eye images with the iris of various colors (NICE.II training dataset, 2009).

number of SR in the left and right SR searching regions, respectively. The $T_\sigma$ and $T_D$ are the threshold values of the STD and the number of eyelash pixels respectively. The $T_\sigma$ and $T_D$ were experimentally determined, and false classification errors of left and right eyes did not occur.

In case that an input image is determined as "left eye" class, it is matched with only the enrolled images of left eyes. If it is determined as "right eye" class, it is matched with only the enrolled images of the right eyes. In case that an input image is determined as "undetermined eye" class, it is matched with all the enrolled images of the left or right eye.

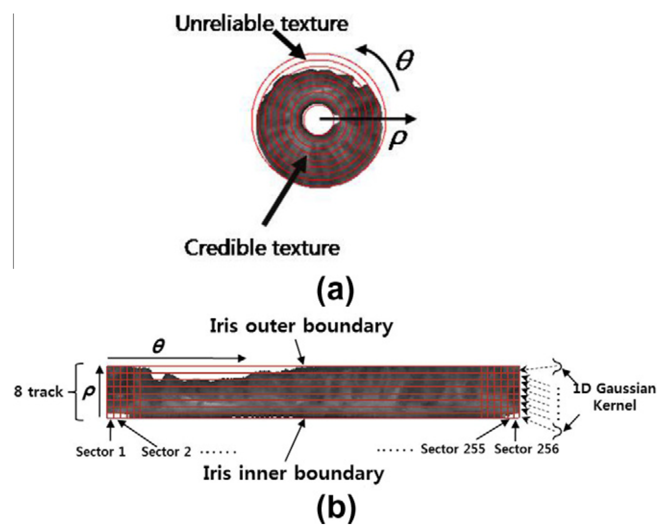


**Fig. 9.** An example of the size normalization. (Park and Park, 2007) (a) Segmented iris region. (b) Normalized image of 256 × 8 pixels of (a).

### 2.4. Pre-classification based on RGB channels

As shown in Fig. 8, different colors are observed in some human eyes. Each pixel of the iris region has three components—red, green, and blue. Among the three components, we select the highest value per pixel. For example, if the red value is higher than green or blue value, the pixel is determined as being a red pixel.

Then, the ratio of "the number of red pixels in iris region" to "the total number of pixels in iris region" is defined. By using the same rule, we can obtain the two ratios and of the green and blue pixels in the iris region, respectively. Finally, the input iris image is determined to be an imposter data by the following rules:

$$\begin{array}{ll} I, & \mathit{if}\ (|R_E - R_R| \geqslant T_R)\ \mathit{or}\ (|G_E - G_R| \geqslant T_G)\ \mathit{or}\ (|B_E - B_R| \geqslant T_B) \\ NC, & \mathit{Otherwise} \end{array} \tag{8}$$

where $R_E$, $G_E$ and $B_E$ are the ratios of red, green and blue pixels in the enrolled iris image, respectively. In addition, $R_R$, $G_R$ and $B_R$ are the ratios of red, green and blue pixels in an input image, respectively. The $T_R$, $T_G$ and $T_B$ are the threshold values of the ratios, which are empirically determined, with which false rejection errors do not occur. The $I$ represents "rejected as Imposter data". The $NC$ represents "go to the Next Classification step" ("5" of Fig. 2 and Section 2.6).

### 2.5. Generating the normalized 256 × 8 pixel image

The human iris has individual variations in diameter. And the length of the inner boundary of the iris varies with contraction and dilation of the pupil area due to variation in illumination. In

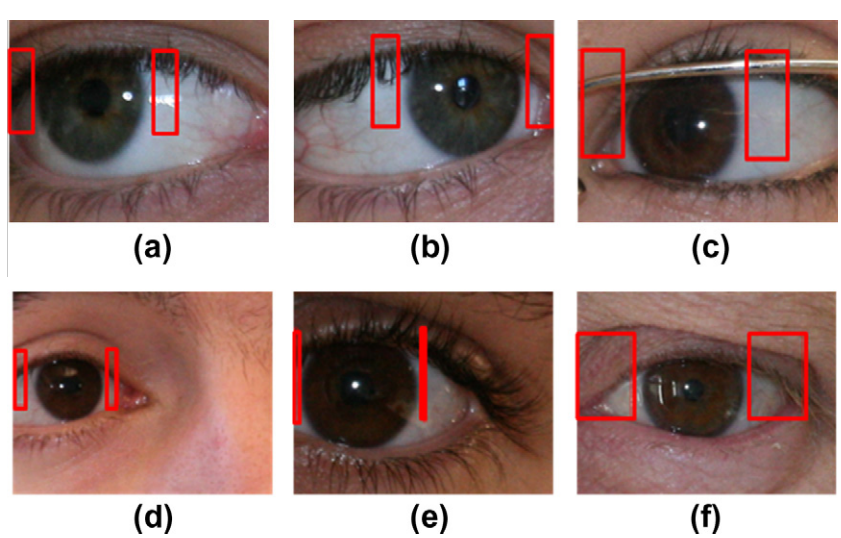

**Fig. 10.** Examples of the "undetermined eye" class.

addition, the iris size in image can be affected by the Z-distance between the camera and human eye. Therefore, the size normalization is required before measuring the dissimilarity in the color space channels and extracting iris codes.

The detected iris region in Cartesian coordinates (Fig. 9a) is transformed into that of polar coordinates (Fig. 9b) for the size normalization. The iris image of polar coordinates $(\rho, \theta)$ is divided into 8 tracks and 256 sectors as shown in Fig. 9b (Park and Park, 2007). In each track, the pixel values are averaged in the vertical ($\rho$ axis) direction by using a one-dimensional (1-D) Gaussian kernel. Consequently, a normalized iris image of $256 \times 8$ pixels is produced as shown in Fig. 9b (Park and Park, 2007).

### 2.6. Extracting ED, CSD, and HD scores in color space channels

The dissimilarity between an input and the enrolled images is calculated in the color space models such as RGB (Boyce, 2006), YIQ, YUV, YCbCr, HSI and CMY. The Euclidean distance (ED), chi square distance (CSD), and hamming distance (HD) are used to measure the dissimilarity in each color space channel with the normalized image. The ED is calculated as (Gonzalez and Woods, 2002):

$$E = \frac{1}{MN}\sqrt{\sum_{x=0}^{M-1}\sum_{y=0}^{N-1}(P(x,y) - Q(x,y))^2} \tag{9}$$

where $P(x,y)$ and $Q(x,y)$ denote the values of the color channels at the $(x,y)$ position of the enrolled image and an input image, respectively. Because the ED is calculated in the normalized image of Fig. 9b, $M$ and $N$ are 256 and 8, respectively.

The CSD represents dissimilarity between two histograms of color space channels. After calculating the two histograms of the color space channel in the normalized enrolled and input images, respectively, the CSD is calculated as (The OpenCV Reference Manual, 2011):

$$C = \sum_{k=0}^{B}\left(\frac{(e_k - r_k)^2}{e_k + r_k}\right) \tag{10}$$

where $e_k$ and $r_k$ each represent the frequencies of the $k$th bin in two histograms of each color space channel of the enrolled image and an input image, respectively.

The HD is calculated from the binary code extracted by a Gabor wavelet filter (see Section 2.7). The 6 sets of binary codes are extracted in the RGB, YIQ, YUV, YCbCr, HSI and CMY channels, respectively.

The input images are classified into genuine and imposter matching by the conditions as:

$$\begin{array}{ll} G, & \textit{if } (T_i^{E.\min} > E_i) \textit{ or } (T_i^{C.\min} > C_i) \textit{ or } (T_i^{H.\min} > H_i) \\ I, & \textit{if } (T_i^{E.\max} < E_i) \textit{ or } (T_i^{C.\max} < C_i) \textit{ or } (T_i^{H.\max} < H_i) \\ NC, & \textit{Otherwise} \end{array} \tag{11}$$

where $E_i$, $C_i$ and $H_i$ mean the ED, CSD and HD calculated from the color space channels, respectively; the $i$-subscript means the each channel of RGB, YIQ, YUV, YCbCr, HSI and CMY. $T_i^{E.\min}$, $T_i^{C.\min}$ and $T_i^{H.\min}$ represent the threshold values of ED, CSD and HD. These three thresholds were empirically obtained, with which false acceptance errors do not occur. $T_i^{E.\max}$, $T_i^{C.\max}$ and $T_i^{H.\max}$ are also empirically determined, with which false rejection errors do not occur. The $G$ and $I$ mean "accepted as Genuine data" and "rejected as Imposter data", respectively. The $NC$ represents "go to the Next Classification step" ("9" of Fig. 2 and Section 2.8).

The extracted 256 bits in each track are matched by bit-shifting. Among the multiple HD scores calculated from matching by bit-shifting, the lowest HD is determined as final dissimilarity score (Park and Park, 2007). Since the horizontal width (256 pixels) of the normalized image represents the whole boundary of iris region (of 360°), and the bit is extracted from each pixel position of 256 pixels, the bit is regarded as being extracted per 1.4° (360°/256), consequently. So, matching with one bit shifting can handle the rotation of 1.4° of iris image (Park and Park, 2007).

And the chi square distance (CSD) is used as shown in Eq. (10), which calculates the two histograms of the color space channel in the normalized enrolled and input iris images. Since it calculates the dissimilarity between two iris images based on the histogram information of color, it is robust to the rotation variations of iris images. In case of the off-angle data as shown in Fig. 10a–c, left or right-side iris region is squeezed whereas the other side region is stretched in the input image. However, we normalize the squeezed (or stretched) iris region into the rectangular shape of $256 \times 8$ pixels before extracting iris codes for matching considering the problem of the off-angle data.

Various color descriptors (including color space, color quantization, dominant colors, color structure etc.) are used in MPEG-7 (MPEG7 color descriptors, 2004). In color space of MPEG-7, RGB, YCbCr, HSV and monochrome, etc. are used. And our color classification strategy based on RGB, YCbCr, and HSI can be regarded as MPEG-7 color descriptor. And chi square distance (CSD) which calculates the two histograms of the color space channel in the normalized enrolled and input iris images is used as shown in Eq. (10), and the colour structure descriptor of MPEG-7 includes colour content (like colour histogram) and information of the content's structure (MPEG7 colour descriptors, 2004).

### 2.7. Extracting iris code in Gray channels

This section corresponds to "8" of Fig. 2 and we use "textural information" of iris region for matching. Iris binary codes are extracted from gray channel and HD is calculated. Since the two HDs from red and green channels are already calculated in previous step (Section 2.6), the three HDs from gray, red and green channels are combined by weighted SUM rule (see Section 2.8). In our experiment, the blue channel is excluded because the accuracy of iris recognition in the blue channel is low. With the normalized image of $256 \times 8$ pixels of Fig. 9b, a 1-D Gabor wavelet filter (25 kernel size and 1/20 frequency) is used to extract the binary iris codes (Park and Park, 2007). The optimal kernel size and frequency were obtained by experiments in terms of recognition accuracy. In each track (of 8 tracks), the convolution of the intensity channel with the 1-D Gabor wavelet filter is performed in the horizontal ($\theta$ axis) direction. The horizontal width of the normalized image is 256 pixels and the convolution with the 1-D Gabor filter is performed at each pixel position in the horizontal direction of each track. Consequently, the 256 magnitude values by the 1-D Gabor filtering are obtained in each track (Park and Park, 2007). If the magnitude value is greater than (or same to) 0, "1" is assigned. If not, "0" is assigned. Consequently, 256 bits are obtained in each track (of 8 tracks), and total 2048 bits (256 bits/track $\times$ 8 tracks) are obtained from the normalized image of $256 \times 8$ pixels (Park and Park, 2007).

The normalized image contains the region occluded by the specular reflection (SR), eyelid and eyelashes. To exclude the iris code extracted from the occluded region for matching, the mask code of 2048 bits is also used, which represents whether the corresponding iris code is extracted from occluded region or not. Only the iris codes that are extracted from un-occluded region are used for calculating the HD (Daugman, 2003, 2004; Park and Park, 2007).

### 2.8. Extracting final matching score using weighted SUM rule

The three HD scores of the red, green and gray channels are combined by the weighted SUM rule as follows:

$$O_{HD} = w_{red} \times S_{red} + w_{green} \times S_{green} + w_{gray} \times S_{gray} \quad (12)$$

where $S_{red}$, $S_{green}$ and $S_{gray}$ represent the HD scores of the red, green and gray channels, respectively. The $w_{red}$, $w_{green}$ and $w_{gray}$ represent the optimal weights of red, green and gray HD scores, respectively. The optimal $w_{red}$, $w_{green}$ and $w_{gray}$ were empirically determined as 0.4, 0.4 and 0.2, respectively.

## 3. Result analysis

For experiments, the NICE.II training data set selected from UBIRIS.v2 database was used, which is composed of 1000 images including 171 classes (NICE.II training dataset, 2009) (Proença et al., 2010). The image quality of this database was extremely degraded by various noise factors as shown in Fig. 1. The image resolution is $400 \times 300$ pixels including RGB color channels. In our experiments, the number of authentic tests was 3593 and the number of imposter tests was 495,907. The number of "left eye" and "right eye" in the NICE.II training data set are 491 and 509 images, respectively. The decidability value is used to evaluate separability between authentic and imposter distributions. The decidability value is measured as (NICE.II training dataset, 2009):

$$d' = \frac{|\mu_A - \mu_I|}{\sqrt{\frac{\sigma_A^2 + \sigma_I^2}{2}}} \quad (13)$$

where $\mu_A$ and $\mu_I$ denote the mean of the authentic and imposter distributions, respectively, and $\sigma_A$ and $\sigma_I$ denote the standard deviation of the authentic and imposter distributions, respectively.

As the 1st step classification, the "left eye" and "right eye" classes are discriminated by using the eyelash distribution and the number of SR regions. Table 1 shows the accuracy of the classification.

The number of "left eye" and "right eye" in the NICE.II training data set are 491 and 509 images, respectively. We could obtain the classification accuracy of 90.9% as shown in Table 1 while false classification errors did not occur. The false classification error means that the "left eye" image is incorrectly classified as the "right eye" or the "right eye" image is incorrectly classified as the "left eye". The "undetermined" means that an image could not be classified into the "left eye" or "right eye" classes by using the eyelash distribution and the number of SR. The images of the third class (undetermined) are compared against all left and right eye images by the 2nd and 3rd step classifications of Fig. 2.

Fig. 10 shows the examples of the "undetermined eye" class. In the case where the iris is very close to the left or the right position of eye corner as shown in Fig. 10a and b, the searching region used to check the eyelashes was so small that enough information of eyelashes was not obtained. Consequently, the image could not be determined as the "left eye" or "right eye". An image was also determined as the "undetermined eye" in case the glasses occluded the eyelashes as shown in Fig. 10c. In addition, the partially captured eye image decreased the searching region of eyelashes (in shown Fig. 10d and e). Since the gray levels of eyelashes in Fig. 10f are higher than our predetermined threshold and the eyelashes are not detected, the image in Fig. 10f is determined as "undetermined eye".

**Table 1**
The accuracy of classification of "left eye" and "right eye".

| | Correct (%) | Undetermined (%) |
|---|---|---|
| Left eye | 87.98 (432/491 images) | 12.02 (59/491 images) |
| Right eye | 93.71 (477/509 images) | 6.29 (32/509 images) |
| Total | 90.9 (909/1000 images) | 9.1 (91/1000 images) |

In the pre-classification based on RGB channels ("3" of Fig. 2 and Section 2.4), iris images are discriminated by the ratio of red, green, and blue pixels. However, the color information of iris images of same person can be differently observed by the illumination as shown in Fig. 11. So, in our research, the thresholds of pre-classification were determined considering these variations of iris colors of same person.

Table 2 shows the comparisons of EER and decidability value of the proposed method with pre-classification to the previous method without pre-classification. In the previous method without pre-classification (Park and Park, 2007), the iris code of 2048 bits and the mask code of 2048 bits were extracted from the normalized gray image of $256 \times 8$ pixels, as shown in Section 2.7. The 1-D Gabor filter was used for the extraction of iris codes, and any color information or pre-classification of Fig. 2 was not used. For measuring dissimilarity, HD was used (Park and Park, 2007).

The EER of the previous method was 25.7% and the EER of the proposed method was 16.942%. In addition, the decidability value was increased as much as 0.3405 (1.6398 − 1.2993). The accuracy of the proposed method (the decidability value of 1.6398) is the 4th highest rank in NICE.II contest (NICE.II training dataset, 2009).

As shown in Table 2, the increase of EER in case of the method without the 1th step classification of Fig. 2 is about 16.9% ($100 \times ((19.807 - 16.942)/16.942)$) compared to the proposed method with all the pre-classification steps of Fig. 2. The increase of EER in case of the method without the 2nd step classification of Fig. 2 is about 1.8% ($100 \times ((17.242 - 16.942)/16.942)$) compared to the proposed method with all the pre-classification steps of Fig. 2. The increase of EER in case of the method without the 3rd step classification of Fig. 2 is about 1.4% ($100 \times ((17.182 - 16.942)/16.942)$) compared to the proposed method with all the pre-classification steps of Fig. 2. From them, we can know that the effect by the 1st classification step on the final accuracy of iris recognition is much larger than the 2nd and 3rd classification methods. And that by the 2nd classification step is a little larger than the 3rd classification method.

In case of measuring accuracy only with 491 left iris images (the numbers of authentic and imposter tests are 1731 and 118,564, respectively), the numbers of false rejection and false acceptance cases are 341 and 23,876, respectively. In case of measuring accuracy only with 509 right iris images (the numbers of authentic and imposter tests are 1862 and 127,424, respectively), the numbers of false rejection and false acceptance cases are 387 and 25895, respectively. In case of measuring accuracy with 1000 left and right iris images (the numbers of authentic and imposter tests are 3593 and 495,907, respectively), the numbers of false rejection and false acceptance cases are 614 and 83,291, respectively. Since the results with 491 left iris images (or 509 right iris images) are obtained by separating the left and right irises manually, they do not include the errors of the 1st classification (the classification between left and right irises). So, by comparing the result with both irises

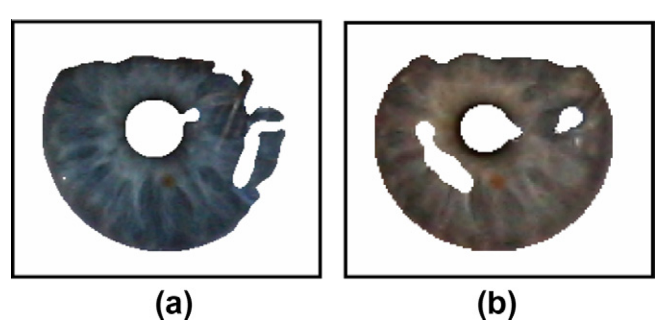

**Fig. 11.** Iris images of same person having different color information.

**Table 2**
The iris recognition accuracy in terms of equal error rate (EER) (%) and decidability value.

| Method | EER (%) | Decidability value |
|---|---|---|
| Previous method without pre-classification (Park and Park, 2007) | 25.7 | 1.2993 |
| The method without the 1st step classification of Fig. 2 | 19.807 | 1.4954 |
| The method without the 2nd step classification of Fig. 2 | 17.242 | 1.6213 |
| The method without the 3rd step classification of Fig. 2 | 17.182 | 1.6272 |
| Proposed method with all the pre-classification steps of Fig. 2 (on both right and left eye images) | 16.942 | 1.6398 |

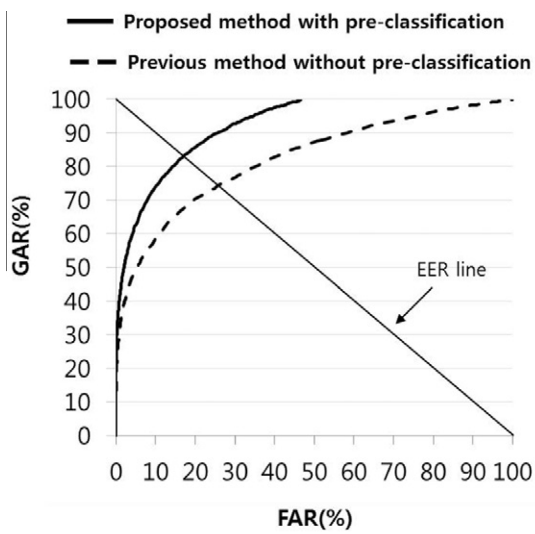


**Fig. 12.** ROC curves of proposed method with pre-classification and previous method (Park and Park, 2007) without pre-classification.

**Table 3**
Processing time.

| | Processing time (ms) |
|---|---|
| Detection of pupil and iris region | 48.1 |
| Pre-classification of the left or right eye | 69.2 |
| Pre-classification based on RGB channels | 1 |
| Generating the normalized images of 256 × 8 pixels | 263 |
| Extracting ED, CSD, and HD values of color space channels | 1 |
| Extracting iris code and calculating HDs in gray, red and green channels | 43.8 |
| Obtaining final HD score using weighted SUM rule | 1 |
| Total | 427.1 |

(1000 iris images), the numbers of false rejection cases with 491 left and 509 right iris images are reduced as 273 (614 − 341) and 227 (614 − 387), respectively. In addition, by comparing the result with both irises, the numbers of false acceptance cases with 491 left and 509 right iris images are much reduced as 59,415 (83,291 − 23,876) and 57,396 (83,291 − 25,895), respectively.

Fig. 12 shows the receiver operational characteristic (ROC) curves with the genuine acceptance rate (GAR) (100 − FRR (%)) at a variable false acceptance (FAR). FRR is the error rate of rejecting a genuine user as an imposter one and the false acceptance rate (FAR) is the error rate of accepting an imposter user as a genuine one (Ratha and Govindaraju, 2008). The recognition accuracy of the proposed method with pre-classification is higher than that without pre-classification as shown in Fig. 12. In the final experiment, we measured the processing time of the proposed method on a desktop computer with Intel Core I7 processor of 3.33 GHz and 4 GB RAM. As shown in Table 3, the processing time for detection of pupil and iris region, and pre-classification of the left or right eye were 48.1 ms and 69.2 ms, respectively. The processing time for generating the normalized images of 256 × 8 pixels, which were obtained in the each channel of RGB, YIQ, YUV, YCbCr, HSI and CMY, was 263 ms. The processing time for extracting iris code and calculating HDs in gray, red and green channels was 43.8. The total processing time was 427.1 ms.

## 4. Conclusion

We propose a new iris recognition method for the iris images degraded by noisy factors. The genuine and imposter matching are determined by pre-classification including the 1st and 2nd step classifications based on "left or right eye" and "color" information of iris. And the iris authentication is completed by comparing the iris binary code based on "texture information" of iris region. As the experimental results, the decidability value evaluated by the NICE.II contest was 1.6398, and the EER was 16.942%. In future works, we plan to study detection of the medial canthus and the lateral canthus to improve the classification accuracy of the "left eye" and "right eye" images, by which the consequent accuracy of iris recognition can be enhanced.

## Acknowledgments

This work was supported by the National Research Foundation of Korea (NRF) through the Biometrics Engineering Research Center (BERC) at Yonsei University [R112002105070020(2010)] and in part supported by NAP (National Agenda Project) of Korea Research Council of Fundamental Science & Technology.

## References

Boyce, C., Ross, A., Monaco, M., Hornak, L., Li, X., 2006. Multispectral iris analysis: a preliminary study. In: Proc. Computer Vision and Pattern Recognition Workshop on Biometrics.
Daugman, J., 1993. High confidence visual recognition of persons by a test of statistical independence. IEEE Trans. Pattern Anal. Mach. Intell. 15 (11), 1148–1161.
Daugman, J., 2003. The importance of being random: statistical principles of iris recognition. Pattern Recognit. 36 (2), 279–291.
Daugman, J., 2004. How iris recognition works. IEEE Trans. Circuits Syst. Video Technol. 14 (1), 21–30.
Gonzalez, R.C., Woods, R.E., 2002. Digital Image Processing, second ed. Prentice-Hall, NJ.
Jeong, D.S., Hwang, J.W., Kang, B.J., Park, K.R., Won, C.S., Park, D.-K., Kim, J., 2010. A new iris segmentation method for non-ideal iris images. Image Vis. Comput. 28 (2), 254–260.
Lefohn, A., Budge, B., Shirley, P., Caruso, R., Reinhard, E., 2003. An ocularist's approach to human iris synthesis. IEEE Comput. Graph. Appl. 23 (6), 70–75.
Li, Z.-N., Drew, M.S., 2004. Fundamentals of Multimedia. Pearson Prentice-Hall, NJ.
MPEG7 color descriptors, 2004 <http://mpeg.chiariglione.org/standards/mpeg-7/mpeg-7.htm#E11E2> (accessed 19.9.11).
Na, J.I., Kwon, O.S., Kim, B.J., Park, W.S., Oh, J.K., Kim, K.H., Cho, K.H., Eun, H.C., 2006. Ethnic characteristics of eyelashes: a comparative analysis in Asian and Caucasian females. Brit. J. Dermatol. 155 (6), 1170–1176.
Nam, G.P., Kang, B.J., Park, K.R., 2010. Robustness of face recognition to variations of illumination on mobile devices based on SVM. KSII Trans. Internet Inf. Syst. 4 (1), 25–44.
NICE.II training dataset., 2009 <http://nice2.di.ubi.pt/> (accessed 19.9.11).
Park, H.A., Park, K.R., 2007. Iris recognition based on score level fusion by using SVM. Pattern Recognit. Lett. 28 (15), 2019–2028.

Proença, H., Alexandre, L.A., 2007. Toward noncooperative iris recognition: a classification approach using multiple signatures. IEEE Trans. Pattern Anal. Mach. Intell. 29 (4), 607–612.
Proença, H., Filipe, S., Santos, R., Oliveira, J., Alexandre, L.A., 2010. The UBIRIS.v2: a database of visible wavelength iris images captured on-the-move and at-a-distance. IEEE Trans. Pattern Anal. Mach. Intell. 32 (8), 1529–1535.
Ratha, N.K., Govindaraju, V., 2008. Advances in Biometrics: Sensors, Algorithms and System. Springer.
The OpenCV Reference Manual, release 2.3, August 17, 2011.